Vectorial Multistep Electron Transfer at the Gold Electrodes Modified with Self-Assembled Monolayers of Ferrocene−Porphyrin−Fullerene Triads

Hiroshi Imahori,*,†,§ Hiroko Yamada,† Yoshinobu Nishimura,‡ Iwao Yamazaki,*,‡ and Yoshiteru Sakata*,†

The Institute of Scientific and Industrial Research, Osaka University, 8-1 Mihoga-oka, Ibaraki, Osaka 567-0047, Japan, and Department of Molecular Chemistry, Graduate School of Engineering, Hokkaido University, Sapporo 060-8628, Japan

Received: October 25, 1999; In Final Form: December 30, 1999

Self-assembled monolayers of ferrocene−porphyrin−C_{60} triads on gold electrodes were prepared to mimic photosynthetic electron transfer events where efficient conversion of light to chemical energy takes place via the long-lived, charge-separated state with a high quantum yield. Adsorbed amounts of the triads on the gold electrodes, estimated from the charge of the anodic peak of the ferrocene, are comparable to those of the well-ordered porphyrin−alkanethiols and C_{60}−alkanethiols on gold electrodes. The results, together with blocking experiments using a redox probe, indicate that the triad molecules are well-packed with an almost perpendicular orientation on the gold surface. The monolayer thickness obtained using X-ray reflectivity analysis is consistent with the structural model of the monolayer. Photoelectrochemical studies were carried out in a standard three-electrode system using the gold electrodes modified with the self-assembled monolayers of the triads. Stable cathodic photocurrents were observed in the presence of electron carriers such as oxygen and/or methyl viologen in the electrolyte when the modified gold electrodes were illuminated with a monochromic light. A photoinduced multistep electron-transfer mechanism is proposed for the photoelectrochemical cells. Thus, vectorial electron transfer or partial charge transfer occurs from the excited singlet state of the porphyrin to the C_{60}, followed by the successive charge shift from the ferrocene to the porphyrin cation radical, to produce the ferrocene cation radical and the C_{60} anion radical. The C_{60} anion radical gives an electron to the counter electrode via the electron carriers in the electrolyte solution, whereas electron transfer takes place from the gold electrode to the ferrocene cation radical, resulting in the recovery of the initial state and the generation of the overall electron flow. The artificial photosynthetic cells show the highest quantum efficiency (20−25%) ever reported for photoinduced multistep electron transfer at monolayer-modified metal electrodes and across artificial membranes using donor−acceptor linked molecules. The result indicates clearly that C_{60} acts as an excellent electron acceptor as well as an electron mediator in artificial photosynthetic membranes. The molecule-based methodology will provide a new direction for the development of solar energy conversion and molecular devices.

Introduction

The conversion of light to chemical energy is a subject of interest not only in the area of basic research, but also of practical application. Photosynthesis is a natural supramolecular system where the conversion and storage of solar energy take place efficiently. The core of photosynthesis is initial electron transfer (ET) events in the reaction center complex.[1] The ultrafast and unidirectional multistep ET occurs along well-arranged pigments embedded in the transmembrane proteins, leading to the generation of a charge-separated state across the membrane with a quantum efficiency (Φ) of nearly 100%. The importance and complexity of ET reactions in photosynthesis have prompted many organic chemists to design and synthesize donor−acceptor linked systems that mimic the highly efficient multistep ET process. Some of the covalently linked molecular arrays, such as triads, tetrads, and pentads, produce a long-lived, charge-separated state with a high quantum yield,[2] demonstrating that multistep ET is an inevitable strategy for the construction of artificial photosynthesis. However, efficient conversion (overall quantum yield: $\Phi = 1-10\%$) of light to photocurrents or chemical products via the charge-separated state has been hampered, provided that the donor−acceptor linked molecules are incorporated into artificial membranes such as lipid bilayers and Langmuir Blodgett (LB) membranes and/or organized at electrodes.[3−9] This is because it is quite difficult to assemble the donor−acceptor linked molecules unidirectionally in an artificial manner.

Self-assembled monolayers (SAMs)[10] have emerged as an alternative and useful strategy for assembling molecular components on surface. They are formed spontaneously by chemisorption, yielding robust, well-defined structures on substrates. The most well-established systems of SAMs are alkanethiols $CH_3(CH_2)_nSH$ on gold. Alkanethiols with a long methylene chain ($n \geq 10$) are known to form densely packed SAMs on gold surfaces using S−Au linkage. Thus, it is expected that, when a thiol group with a long alkyl chain or an equivalent is introduced at the end of donor−acceptor linked molecules, it would be arranged unidirectionally on the gold electrodes,

* E-mail: imahori@ap.chem.eng.osaka-u.ac.jp; yamiw@eng.hokudai.ac.jp; sakata@sanken.osaka-u.ac.jp.

† Osaka University.

‡ Hokkaido University.

§ Present address: Department of Material and Life Science, Graduate School of Engineering, Osaka University, Suita, Osaka 565-0871, Japan.

10.1021/jp993784f CCC: $19.00
Published on Web 02/16/2000

CHART 1

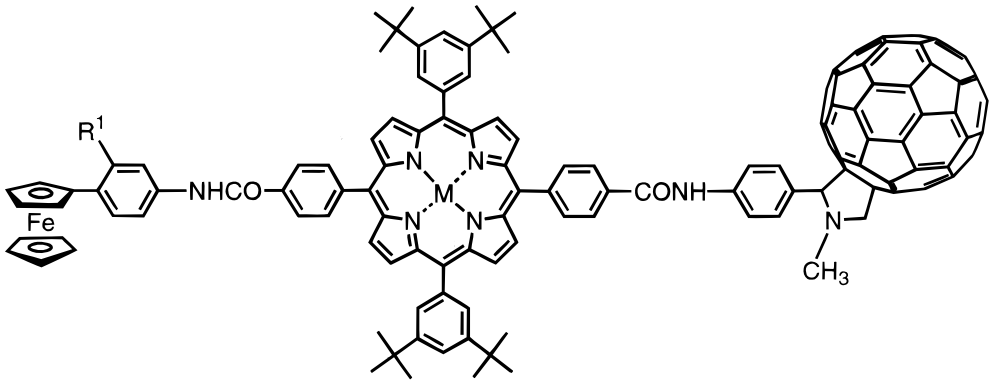

1a: M=H_2; **1b**: M=Zn, R^1=$O(CH_2)_{11}SH$
2a: M=H_2; **2b**: M=Zn, R^1=H

leading to the formation of a uniform, well-ordered SAM. So far there are a few reports of SAMs of donor−acceptor linked dyads on metal electrodes.[11−13]

Fullerenes have appeared as a new electron acceptor in the past decade. The unique three-dimensional structures of fullerenes have fascinated many synthetic chemists to prepare a variety of donor-linked fullerenes for the elucidation of the peculiar ET dynamics in fullerenes.[14−19] We[14b,e,15] and others[17c,20] have found that fullerenes as an acceptor accelerate photoinduced charge separation (CS) as well as charge shift (CSH) and slow down charge recombination (CR). It has been proposed by us that this is a result of the small reorganization energies of fullerenes in ET,[15b,c] which is one of the important controlling factors in ET, such as free energy change, electronic coupling, separation distance, and temperature. In the Marcus parabolic curve, decreasing reorganization energy pushes the CS from the normal region toward the top region, but forces the CR into the inverted region considerably, leading to the optimization of each ET process. This is the same strategy in photosynthetic ET in the reaction center where each ET process is optimized by using the small reorganization energies of chromophores embedded in the protein matrix, in addition to tuning the free energy changes and the electronic coupling between the redox pair. Thus, the utilization of three-dimensional fullerenes as an acceptor in multistep ET systems such as triads, instead of conventional two-dimensional aromatic acceptors, would allow us to realize an artificial multistep ET process with the longer lifetime and the higher quantum efficiency.[1] Bearing these in mind, we designed a ferrocene (Fc)−zinc porphyrin (ZnP)−C_{60} triad **2b** consisting of a linear rigid array of the three chromophores in the sequence of Fc, ZnP, and C_{60} (Chart 1).[15i] On the basis of the redox potentials of the chromophores, the energy levels of the excited and charge-separated states in the triad are in the order of $Fc-{}^1ZnP^*-C_{60}$ > $Fc-ZnP^{\bullet+}-C_{60}^{\bullet-}$ > $Fc^{\bullet+}-ZnP-C_{60}^{\bullet-}$. From the time-resolved transient absorption spectroscopy, we concluded that the triad displays a sequential two-step ET within the molecule: $Fc-{}^1ZnP^*-C_{60}$ → $Fc-ZnP^{\bullet+}-C_{60}^{\bullet-}$ → $Fc^{\bullet+}-ZnP-C_{60}^{\bullet-}$. In addition, it was found that a long-lived, charge-separated state is produced with a high quantum yield. These results have urged us to prepare new triad molecules **1** where a polyalkanethiol is attached to the terminal of the triad moiety (Chart 1). As we mentioned in the former part, the underlying densely packed monolayer of the polyalkanethiols on a gold surface would ensure the orientational array of the triad unit over the polyalkanethiol SAMs. On the basis of the multistep ET strategy, the utilization of C_{60} with small reorganization energy, and the SAM technique, such triad cells would improve the quantum yield greatly, compared with the previous dyad systems. The comprehensive studies on ferrocene-free base porphyrin−C_{60} and ferrocene−zinc porphyrin−C_{60} SAMs on the gold surface will be described in this article. The photodynamics at interface will be discussed in comparison to those of **2** obtained using the time-resolved transient absorption spectroscopy in solutions,[15i] together with the fluorescence lifetime measurements for **1**−**6** both in solution and the gold surface (Charts 1 and 2). The photodynamics of **2a** and **2b** in solutions will be reported elsewhere in detail. The preliminary results on the first preparation and photoelectrochemical properties of the SAM of ferrocene-free base porphyrin-C_{60} triad have already been reported.[15h]

Results

Preparation of Modified Gold Substrates and Photophysical Properties. The SAMs of **1** (hereafter, **1**/Au, where/ represents an interface) were prepared as follows; The gold electrodes with Au(111) surface were dipped into a CH_2Cl_2 solution of **1a** at 25 °C for 20 h under argon atmosphere to protect the thiol against oxidation. After the complete modification, **1a**/Au was rinsed well with CH_2Cl_2 and EtOH, and dried with a stream of argon. The surface-bound porphyrins were metalated in $CHCl_3$ with $Zn(OAc)_2$ for 2 h at 50 °C under argon atmosphere.[21] The resulting **1b**/Au was washed copiously with CH_2Cl_2 and EtOH and dried with a stream of argon.

Figure 1 displays absorption spectra of **2** in THF and **1**/Au in air using transmission mode. The absorption spectra of **2a** and **2b** in THF are essentially a linear combination of the absorption spectra of **5**−**7** (Chart 2), respectively, indicating no evidence for strong interaction between these chromophores. Absorption due to the porphyrin is much stronger relative to the C_{60} and the ferrocene, showing that the porphyrin is a major absorber of photons in **1** and **2**. The Soret band of **1a**/Au and **1b**/Au is broad and red-shifted by 11 and 9 nm, respectively, compared to that of **2a** and **2b** in THF (Table 1). The four porphyrin Q-bands with small molar absorption coefficients on the gold surface could not be detected because of the large background absorption within the range of 500−700 nm. The large background may be explained by the structural change on the gold surface owing to chemical etching and/or squeezing out of gold atoms initiated by adsorption of **1a**.[22] Similar red-shift and broadening of the Soret band were reported for porphyrin SAMs on gold electrodes,[12a,23,24] porphyrins in LB

TABLE 1: Results Obtained Using UV−Visible Absorption Spectroscopy in Transmission Mode, Cyclic Voltammetry, and X-ray Reflectivity and Diffuse Scattering Measurements

system	absorbance[a]	λ_{max}/nm[b]	$\Gamma/10^{-10}$ mol cm^{-2} [e] (molecular area /Å^2 molecule^{-1})	thickness (exptl)/Å[f]	thickness (theor)/Å[h]
1a/Au	0.039	431 (420)[c]	1.9 (86)	51	47
1b/Au	0.047	435 (426)[d]	1.5 (110)	*g*	47

[a] Absorbance at the Soret band. [b] At the Soret band. [c] For **2a** in THF. [d] For **2b** in THF. [e] Surface coverage obtained using cyclic voltammetry. [f] Determined using X-ray reflectivity and diffuse scattering measurements. [g] Not measured. [h] Estimated using CPK model, assuming that the triads are densely packed with a methylene spacer 30° from the surface normal.

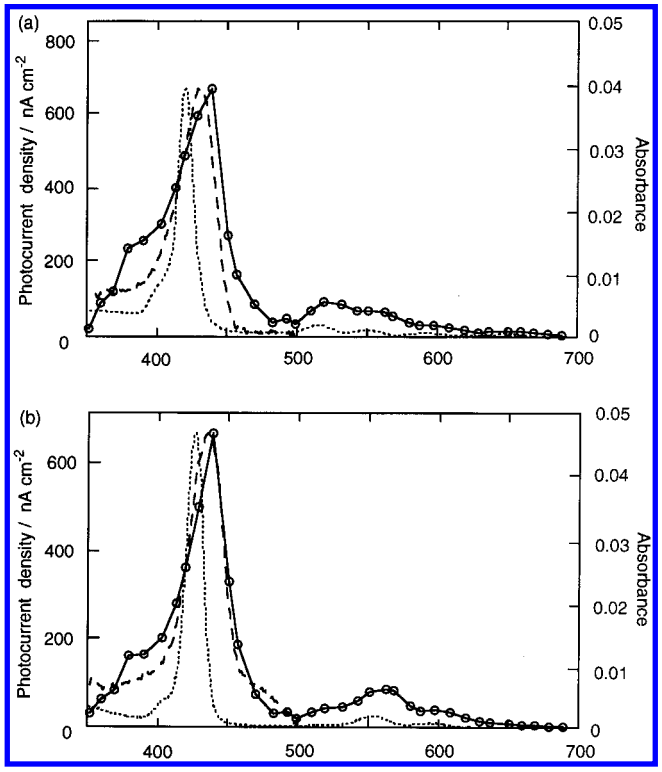

Figure 1. Absorption spectra of (a) **2a** and (b) **2b** in THF (dotted line), (a) **1a**/Au and (b) **1b**/Au in air using transmission mode (dashed line), and action spectra of (a) Au/**1a**/O_2+30 mM MV^{2+}/Pt and (b) Au/**1b**/O_2+30 mM MV^{2+}/Pt cells (solid line with circles); 60 μW cm^{-2}, −200 mV vs Ag/AgCl, O_2-saturated 0.1 M Na_2SO_4 solution containing 30 mM MV^{2+}. The spectra are normalized at the Soret band for comparison.

monolayers on glass and semiconductors,[25] and porphyrin aggregates in solutions.[26] It is well established that a stacked face-to-face porphyrin π-aggregation (sandwich-type H-aggregate) leads to a spectral blue shift relative to the monomer, while side-by-side porphyrin π-aggregation (J-aggregate) leads to a red shift.[26−28] Thus, the relatively small red shift and broadening of the Soret band may be ascribed to the J-aggregate-like partially stacked structures of the porphyrin moieties in the monolayer microenvironment.

Steady-state fluorescence spectra of **2**−**4** in THF have the same band shape and peak positions as those of **5** (**2a**−**5a**: λ_{em}^{max} = 651, 715 nm; **2b**−**5b**: λ_{em}^{max} = 605, 652 nm). No emission from the C_{60} (λ_{em}^{max} = 720 nm) could be detected for **2** and **3**. However, fluorescence spectra of **2** and **3** in THF are quenched strongly as compared to those of **5** when excited at the Soret band under the same concentration (relative intensities: 0.14 for **2a**, 0.19 for **3a**, 0.05 for **2b** and **3b**). In contrast, the relative fluorescence intensity of **4** vs **5** (0.60 for **4a** vs **5a**, 0.37 for **4b** vs **5b**) is much larger, suggesting that quenching of the excited singlet porphyrin (^{1}P*) by the attached C_{60} is a dominant deactivation pathway in **1**. Zinc *meso*-tetraphenylporphyrin (ZnP) is known to be harder to reduce by ca. 0.2 V than the free base porphyrin (H_2P). Thus, the fluorescence quenching experiments show that in **2a** ^1H_2P* is quenched by the C_{60} rather than the ferrocene, whereas in **2b** ^{1}ZnP* is deactivated exclusively by the C_{60}.

CHART 2

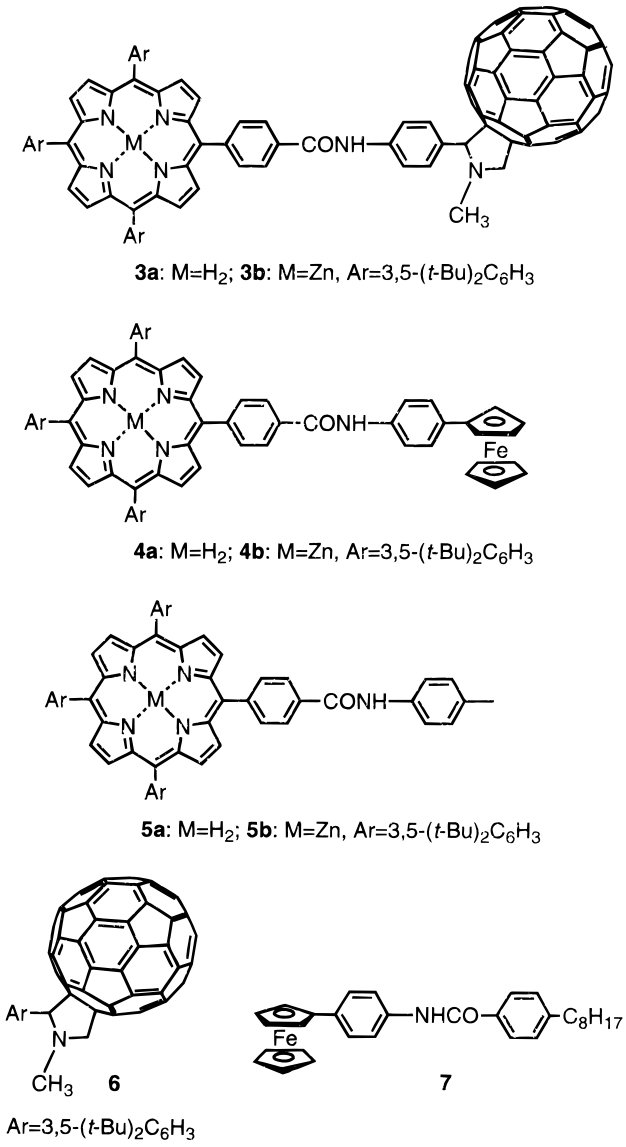

The fluorescence lifetimes of **2**−**5** in benzene and THF and **1**/Au were measured by a picosecond single photon counting technique with excitation at 425 nm, where most of the light is absorbed by the porphyrin, and monitoring at 605 and 655 nm where the emission is due to the zinc porphyrin and the free base porphyrin, respectively. The fluorescence decays of **2a** and **3a** were analyzed to give two components, whereas those of **2b**, **3b**, and **4**−**6** as well as **1**/Au were fitted to give one

TABLE 2: Fluorescence Lifetimes of 2−6 in Benzene and THF and 1/Au

	fluorescence lifetime[a]			
	benzene		THF	
system	τ_1/ns	τ_2/ns	τ_1/ns	τ_2/ns
1a/Au			0.024	
1b/Au			0.022	
2a	1.6 (0.92)	3.9 (0.08)	1.3 (0.95)	3.5 (0.05)
2b	0.21		0.074	
3a	1.8 (0.76)	2.5 (0.24)	1.4 (0.88)	2.7 (0.12)
3b	0.19		0.075	
4a	6.2		5.7	
4b	1.5		1.4	
5a	9.6		9.9	
5b	2.1		2.1	
6[b]	1.4		1.4	

[a] Numbers in parentheses are relative amplitudes of preexponential factors in exponential functions. [b] Monitored at 720 nm.

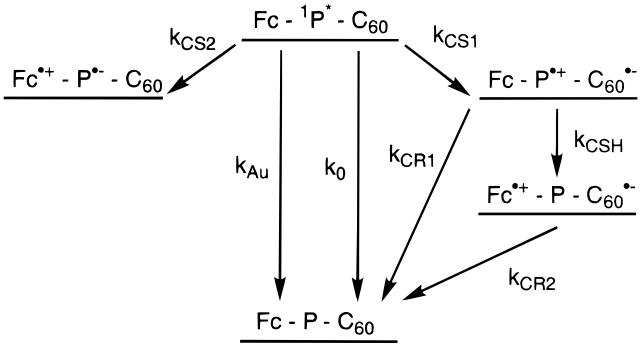

Figure 2. Deactivation pathway of the excited singlet state of the porphyrin in **1**/Au and **2**.

component. The results are summarized in Table 2. These results are quite consistent with those obtained using the steady-state fluorescence studies. We have shown that photoinduced ET produces the ion pair in zinc porphyrin−C_{60} dyads, whereas an exciplex is formed in free base porphyrin−C_{60} dyads.[11b] In addition, photoinduced ET from Fc to ^{1}P* is possible in **2**. Therefore, the emission quenching can be ascribed to photoinduced ET or partial charge transfer (CT) from ^{1}P* to C_{60} and photoinduced ET from Fc to ^{1}P*, as shown in Figure 2. Based on the deactivation scheme for **2a** and **2b** in benzene and THF, rate constants for each process can be calculated (Table 3). Both in **2a** and **2b** k_{CS1} is much faster than k_{CS2} and k_0, showing clearly that the excited singlet state of the porphyrin is quenched by the C_{60} dominantly. It is well known that the excited organic dye on a metal surface is quenched strongly by the metal through energy transfer (EN).[29] The dielectric constant of the LB films made of fatty acids and related compounds is reported to be ca. 2.5.[30] Considering the molecular structures of **1a** and **1b**, the SAMs may be treated as a nonpolar or relatively nonpolar media. Given that the polarity in the monolayers is similar to that in benzene (ϵ = 2.2) and THF (ϵ = 7.58), we can estimate the rate constant (k_{Au}) of the quenching for the excited singlet state of the porphyrin by the gold surface using those for the deactivation in benzene and THF. The value of k_{Au} in **1a**/Au and **1b**/Au is larger than that of k_{CS1} by a factor of 67 and 2.5 in THF and of 91 and 8.3 in benzene, respectively. From these values, the efficiency (Φ_F) for the first CS in the monolayer can be calculated to be 1.6% in THF and 1.2% in benzene for **1a**/Au and 29% in THF and 11% in benzene for **1b**/Au, respectively. These results will be discussed in a comparison with the quantum yield for the photocurrent generation in a later section.

Electrochemical and X-ray Reflectivity Studies. The redox potentials of **2**−**6** were measured by differential pulse voltammetry in a CH_2Cl_2 solution using 0.1 M *n*-Bu_4NPF_6 as a supporting electrolyte (Table 4). The redox potentials of **2** can be roughly explained by the sum of **5**−**7**, implying the weak electronic coupling between the three moieties. Cyclic voltammetric experiments were performed using **1**/Au in the CH_2Cl_2 solution containing 0.1 M *n*-Bu_4NPF_6 electrolyte with a sweep rate of 100 mV s^{-1}. For **1a**/Au and **1b**/Au, two successive waves due to the first oxidations of the ferrocene and the porphyrins were observed, whereas the reduction wave due to the C_{60} was completely irreversible, as shown in Figure 3. The electrochemical behavior is quite similar to that in porphyrin[23] and C_{60} SAMs[31,32] on gold electrodes. Two successive waves due to the first and second oxidations of the porphyrins were clearly seen in the former, whereas the first broad and the second negligible waves due to the first and second reductions of the C_{60} were observed in the latter. An adsorbed amount of **1a**/Au was calculated from the charge of the anodic peak of the ferrocene to be 1.9 × 10^{-10} mol cm^{-2} (= 86 Å^2 molecule^{-1}), which is comparable to those in the well-packed porphyrin−polyalkanethiols (0.8−2.3 × 10^{-10} mol cm^{-2})[12a,c,23] and C_{60}−polyalkanethiols (1.3−2.0 × 10^{-10} mol cm^{-2})[31,32] on gold electrodes (Table 1). Assuming that the triad is densely packed perpendicularly to the gold surface, then the occupied area of one molecule is calculated to be ca. 87 Å^2 for hexagonal packing of the C_{60} moieties, which is consistent with the experimental value. Therefore, we can conclude for **1a**/Au that the triad molecules are well-packed with an almost perpendicular orientation on the gold surface. Similarly, the occupied area of one molecule of **1b**/Au was estimated to be 1.5 × 10^{-10} mol cm^{-2} (= 110 Å^2 molecule^{-1}), which is slightly lower than the value of **1a**/Au. This implies that some porphyrins were lost from the surface of **1b**/Au during metalation.

Figure 4 shows the cyclic voltammetric current−potential (*I*−*V*) responses for a bare gold electrode, **1a**/Au, and **1b**/Au with 1 mM $Fe(CN)_6^{3-}$ as an electroactive species and 1.0 M $NaClO_4$ as an electrolyte.[33] There is a dramatic difference between the *I*−*V* responses for the bare gold and the monolayer-covered electrodes. A reversible cyclic voltammogram of the redox probe was observed for the bare electrode, implying that the redox probe exhibits electrical communication with the bare gold

TABLE 3: Rate Constants for Deactivation Pathways of the Excited Singlet State of the Porphyrin in 1/Au and 2 in Benzene and THF and the Quantum Yields

	rate constant				quantum yield	
system	k_0[a]/10^8 s^{-1}	k_{CS1}[a,b]/10^8 s^{-1}	k_{CS2}[a,b]/10^8 s^{-1}	k_{Au}[c]/10^8 s^{-1}	Φ_F[e]/%	Φ_P[f]/%
1a/Au, **2a**	1.0 (1.0)	6.1 (4.5)	0.74 (0.57)	410 (410)[d]	1.6[c] (1.2)[d]	25
1b/Au, **2b**	4.8 (4.8)	130 (48)	2.4 (1.9)	320 (400)[d]	29[c] (11)[d]	20

[a] **2** in THF. Numbers in parentheses correspond to the values in benzene. [b] $k_{CS} = 1/\tau_1 - k_0 (= 1/\tau_{ref})$. [c] Assuming that each rate constant in the monolayers is identical to that in THF; $k_{Au} = 1/\tau_1 - (k_{CS1} + k_{CS2} + k_0)$. [d] Assuming that each rate constant in the monolayers is identical to that in benzene; $k_{Au} = 1/\tau_1 - (k_{CS1} + k_{CS2} + k_0)$. [e] Efficiency for the first CS in the monolayers; $\Phi_F = (k_{CS1} + k_{CS2})/(k_{CS1} + k_{CS2} + k_{Au} + k_0)$. [f] Quantum yield for the photocurrent generation in the three electrode system at −200 mV vs Ag/AgCl (saturated KCl).

TABLE 4: Electrochemical Results Obtained Using Cyclic Voltammetry and Differential Pulse Voltammetry

	redox potentials/V		
system	$P/P^{\bullet+}$	$Fc/Fc^{\bullet+}$	$C_{60}/C_{60}^{\bullet-}$
1a/Au[a]	1.15 (0.02)	0.51 (0.04)	−0.62[c]
1b/Au[a]	0.91 (0.04)	0.50 (0.06)	−0.62[c]
2a[b]	1.02	0.56	−0.57
2b[b]	0.86	0.52	−0.56
3a[b]	1.04		−0.58
3b[b]	0.86		−0.58
4a[b]	1.02	0.55	
4b[b]	0.88	0.53	
5a[b]	1.02		
5b[b]	0.88		
6[b]			−0.61
7[b]		0.57	

[a] Measured by cyclic voltammetry in CH_2Cl_2 containing 0.1 M *n*-Bu_4NPF_6 with a sweep rate of 100 mV s^{-1} using a Ag/AgCl (saturated KCl) reference. The peak separation between the anodic and cathodic peaks is given in parentheses. [b] Measured by differential pulse voltammetry in CH_2Cl_2 containing 0.1 M *n*-Bu_4NPF_6 with a sweep rate of 20 mV s^{-1} using a Ag/AgCl (saturated KCl) reference. [c] The value of a similar C_{60} SAM[31b] is tentatively used because of the irreversible peak of the C_{60} moiety in **1**/Au.

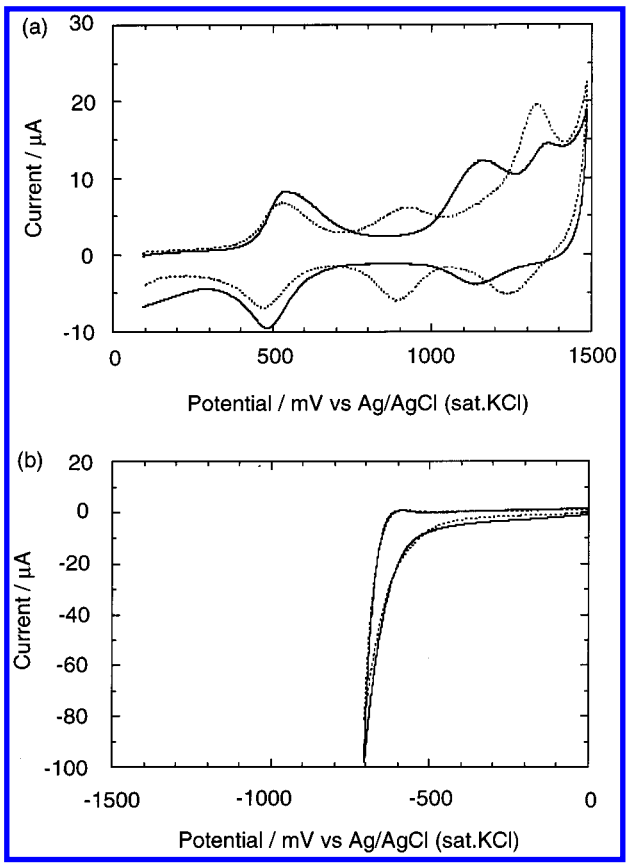

Figure 3. Cyclic voltammograms of **1a**/Au (solid line) and **1b**/Au (dotted line) in CH_2Cl_2 containing 0.1 M *n*-Bu_4NPF_6. The sweeps are shown in (a) oxidation region and (b) reduction region; sweep rate, 100 mV s^{-1}; electrode area, 0.48 cm^2.

electrode. In contrast, such communication decreases apparently for **1a**/Au and becomes irreversible. These data clearly show that the redox communication of $Fe(CN)_6^{3-}$ is interfered by the triad SAM of **1a** due to the densely packed structures. When **1b**/Au was employed, the blocking behavior was not complete, which is quite consistent with the decreased surface coverage for **1b**/Au, in addition to the slightly smaller red shift of the Soret band for **1b**/Au over **1a**/Au.

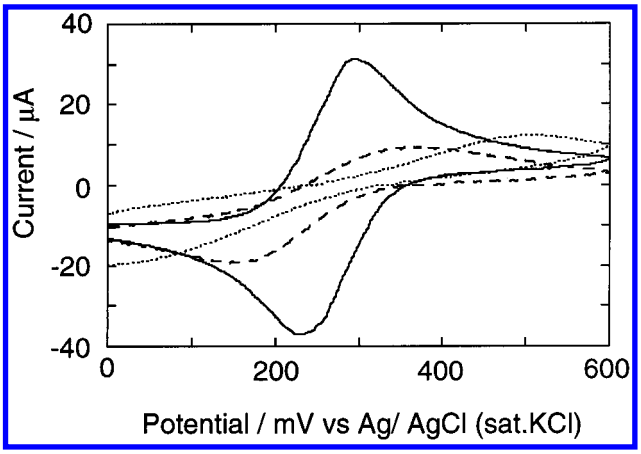

Figure 4. Cyclic voltammograms of bare Au (solid line), **1a**/Au (dotted line), and **1b**/Au (dashed line) in the presence of 1 mM $K_3[Fe(CN)_6]$ in 1.0 M $NaClO_4$; sweep rate, 10 mV s^{-1}; electrode area, 0.48 cm^2.

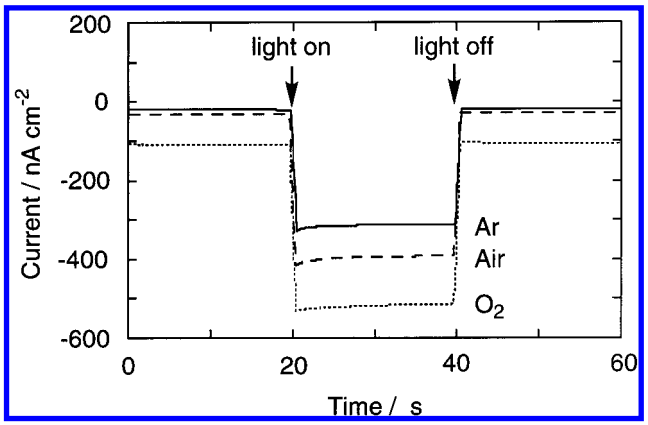

Figure 5. Photoelectrochemical response of Au/**1b**/Pt cell in air-saturated (dashed line), Ar-saturated (solid line), and O_2-saturated (dotted line) 0.1 M Na_2SO_4 solution; λ = 438.5 nm (60 μW cm^{-2}), −200 mV vs Ag/AgCl (saturated KCl).

The thickness of the SAM was measured by X-ray reflectivity.[34] The determined thickness for **1a**/Au is 51 Å, indicating the formation of the monolayers (Table 1). Assuming that the triad molecules are densely packed in the monolayer where the methylene spacer and the triad moiety are aligned at an angle of 30° and 0° from the surface normal, respectively, the thickness of **1**/Au is estimated to be 47 Å using the CPK model. The good agreement between these values strongly supports the well-packed and orientational structure in **1**/Au.

Photoelectrochemical Studies. Photoelectrochemical measurements using **1a**/Au and **1b**/Au in an O_2-saturated 0.1 M Na_2SO_4 solution were carried out in a three-electrode system, which is identical to the previously reported one for evaluating photoinduced multistep ET at monolayer-modified metal electrode (hereafter, Au/**1a**/O_2/Pt and Au/**1b**/O_2/Pt cells).[12a,c] Figure 5 displays time profile of the photoelectrochemical response of Au/**1b**/Pt cell with 438.5 (± 4.9) nm light of 60 μW cm^{-2} on bias voltage of −200 mV vs Ag/AgCl. The SAM showed a cathodic photoelectrochemical response when the light was switched on and off. The cathodic photocurrent decreased significantly by Ar bubbling into the solution, compared with that under the air-saturated conditions. On the other hand, intensity of the photocurrent increased by successive oxygen bubbling, and then recovered to the state under the Ar-saturated conditions by the following Ar bubbling into the solution. It is well known that O_2 acts as an electron acceptor in the similar photoelectrochemical cells.[35] Thus, the results indicate that $C_{60}^{\bullet-}$ gives an electron to O_2 to produce $O_2^{\bullet-}$. When methyl viologen

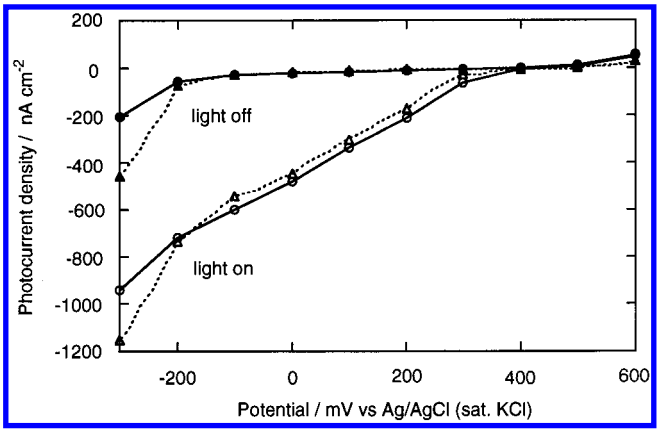

Figure 6. Photocurrent vs applied potential curves for Au/**1a**/O_2+30 mM MV^{2+}/Pt (solid line) and Au/**1b**/O_2+30 mM MV^{2+}/Pt (dotted line) cells when the light is on (white circles and triangles) and off (black circles and triangles): $\lambda = 438.5$ nm (60 μW cm^{-2}), O_2-saturated 0.1 M Na_2SO_4 solution containing 30 mM MV^{2+}.

(MV^{2+}) was employed as an electron carrier, time profile of the photocurrent was dependent on the concentration of MV^{2+}. The initial and stable photocurrents increased with an increase of the MV^{2+} concentration under the Ar- or O_2-saturated conditions, implying that MV^{2+} also accepts an electron from $C_{60}^{\bullet-}$ to generate $MV^{\bullet+}$. As the concentration of MV^{2+} increased under the O_2-saturated conditions, the cathodic photocurrent increased by ca. 20−30% and became saturated at around 30 mM MV^{2+}. There is a good linear relationship between the intensities of the photocurrent and the light (from 10^{-3} to 10 mW cm^{-2}) at each wavelength. The photocurrent was maintained almost constant during the irradiation at least 2 h. The intensity of the photocurrent in the present system is larger by 2 orders of magnitude than that of the previously reported porphyrin−polyalkanethiol SAM systems under the same conditions,[23] implying that the C_{60} and the ferrocene moieties are responsible for the higher efficiency. An increase in the cathodic photocurrent with an increase of the negative bias to the gold electrode, demonstrates that the photocurrent flows from the gold electrode to the counter electrode through the SAM and the electrolyte. The current-applied potential curves of Au/**1a**/O_2+30 mM MV^{2+}/Pt and Au/**1b**/O_2+30 mM MV^{2+}/Pt cells are shown in Figure 6. The cathodic photocurrent dramatically increased, compared with the dark current, as the potential became lower than +500 mV, which is in good agreement with the first oxidation potential of the ferrocene (+500−510 mV ($Fc/Fc^{\bullet+}$)). This indicates that the photocurrent generation is controlled by the ET rate between the gold electrode and the ferrocene, similar to the porphyrin-ferrocene dyad SAM system reported by Uosaki et al.[12a,c] Because the phenyl group at the ferrocene moiety is conjugated to the ferrocene, ET takes place efficiently from the gold electrode to the porphyrin via the ferrocene. When the potential was more positive than +600 mV, the dark current was unstable. On the other hand, the dark current dramatically increased as the applied potential dropped below −200 mV. The action spectra of Au/**1a**/O_2+30 mM MV^{2+}/Pt and Au/**1b**/O_2+30 mM MV^{2+}/Pt cells roughly agree with the absorption spectra of **1a**/Au and **1b**/Au in air, showing that the porphyrin is a major photoactive species for the photocurrent generation (Figure 1). Whitten et al. reported that the action spectrum in the electrolyte solution is different from the absorption spectrum on the electrode in air due to the difference in the aggregation of the squaraine chromophore between the two states.[8] The slight difference of shape and the peak position between the two spectra in our systems may be ascribed to the difference between the real spectra on gold surface in the electrolyte solution and the actual spectra obtained using transmission mode in air as well as to an experimental error depending on the resolution of the interference filters.

Uosaki et al. reported the photoelectrochemical cell of porphyrin−ferrocene SAM, which showed the highest quantum efficiency ($\Phi_P = 12\%$) ever reported for photoinduced multistep ET at monolayer-modified metal electrodes.[12a,c] The quantum yields in the two systems can be compared under the same conditions using the three electrode systems (−200 mV vs Ag/AgCl). Quantum efficiency based on the number of photons absorbed by **1** on the gold electrode was calculated using the input power (438.5 (± 4.9) nm light of 60 μW cm^{-2}), the photocurrent density, and the absorbance on the gold electrode. Under the optimal conditions using the O_2-saturated solution with 30 mM MV^{2+}, we obtained a net photocurrent density of 660 nA cm^{-2} both for Au/**1a**/O_2+MV^{2+}/Pt cell and Au/**1b**/O_2+MV^{2+}/Pt cells at −200 mV. Thus, given an absorbance of 0.059 for **1a**/Au and 0.071 for **1b**/Au, including the reflection at 438.5 nm, the quantum yields (Φ_P) of Au/**1a**/O_2+30 mM MV^{2+}/Pt cell and Au/**1b**/O_2+30 mM MV^{2+}/Pt cells are found to be 25% and 20% (Table 3), respectively. These values are about two times larger than that reported by Uosaki et al. Accordingly, this (25%) is the highest value for photoinduced multistep ET at the monolayer-modified metal electrodes and across the artificial membranes using donor−acceptor linked molecules under the similar conditions.[3−13,23,31,35−37]

Discussion

UV−visible absorption spectroscopy in transmission mode and electrochemical studies, as well as X-ray reflectivity measurements have established the structure of the ferrocene−porphyrin−C_{60} triad monolayers. All of the experiments support the well-ordered, densely packed structure of **1a**/Au, while **1b**/Au has less ordered structure on the basis of the results. It is interesting to compare the present system with the simple porphyrin SAMs, where *meso*-tetraphenylporphyrin with six bulky *tert*-butyl groups at the meta positions of the phenyl rings is linked to the gold surface via methylene spacer (number of the methylenes: $n = 1-7$, 10, 11).[23] The red shift of the Soret band (**1a**: 11 nm; **1b**: 9 nm) in **1**/Au relative to **2** in THF is large by 4−2 nm, compared to the shift (7 nm) of the densely packed porphyrin SAM with a long methylene spacer ($n \geq 10$) on gold electrodes. The value of surface coverage (1.5×10^{-10} mol cm^{-2}) in the porphyrin SAMs ($n = 10$, 11) is identical to that of **1b**/Au and slightly smaller than that of **1a**/Au. The porphyrin moiety in **1**/Au and in the simple porphyrin SAMs has four and six *tert*-butyl groups at the *meso*-phenyl rings of the porphyrin, respectively. Accordingly, owing to the difference of the steric hindrance as a result of the bulky *tert*-butyl groups, the porphyrin moieties in **1**/Au interact much more strongly than those in the simple system, leading to the larger red shift of the Soret band.

The photoelectrochemical performance of the present system can be compared to those of our previous systems under similar three electrode conditions. In the simple porphyrin SAM cells, the photocurrent generation mechanism was explained as follows.[23] The excited singlet state of the porphyrins gives an electron to electron carriers such as O_2 and MV^{2+}, followed by the electron migration to the counter electrode, while ET occurs from the gold electrode to the resulting porphyrin cation radical, leading to the production of the cathodic electron flow. With increasing the number of the methylene spacers ($n = 1-7$, 10, 11) between the gold electrode and the porphyrin, the quantum

yields (ca. 0.1−0.3%) of the simple porphyrin SAM cell at −200 mV vs Ag/AgCl (λ_{ex} = 428.8 nm) increase and reach the maximum value (n = 6) and then start decreasing slightly. The parabolic trend of the quantum yields as a function of the spacer lengths can be interpreted reasonably by the competition between the EN quenching of the excited singlet state of the porphyrin by the gold electrode and the ET quenching by the electron carriers as well as dependence of the ET rate between the gold electrode and the resulting porphyrin cation radical upon the spacer lengths. As the number of the methylene groups increases, both the EN rate of quenching by the gold electrode and the ET rate from the gold electrode to the porphyrin cation radical decrease. Thus, when the spacer lengths become longer, the efficiency for the first CS from ^{1}P* to the diffusing electron carriers increases, whereas that for the CSH from the gold electrode to P$^{\bullet+}$ is reduced, thus giving rise to the offset between the two effects. The quantum yields (20−25%) of the present system under the same conditions are about 2 orders of magnitude larger than those of the porphyrin SAM cells, showing a great contribution of the ferrocene and the C_{60} for the higher quantum yields, as we described before. The quantum yields of the present system are not optimized at the present, but based on the previous results of the porphyrin SAM cells, the utilization of suitable length of the spacers would improve them considerably.

We have also reported the photoelectrochemical cells of C_{60} SAMs on gold electrodes where three isomers of the C_{60} molecules are connected to the gold surface via a long methylene spacer (n = 10).[31] The excited triplet state of the C_{60} is quenched by an electron sacrificer such as ascorbic acid, followed by the ET from the resulting C_{60} anion radical to the gold electrode, producing the overall anodic electron flow. The quantum yields (ca. 7−10%) at +100 mV vs Ag/AgCl (λ_{ex} = 403 nm) in the three electrode system are much improved compared to the simple porphyrin SAM cells, indicating that C_{60} is a good electron acceptor as well as an electron carrier. However, the quantum yields are still 1/4−1/2 times smaller than the present system, implying that a combination of C_{60} with a suitable donor and a sensitizer such as the present system is very effective for the improvement of the quantum yield. This is also supported by the fact that the quantum yields of the present system are about two times larger than that (12% at −200 mV Ag/AgCl in the three electrode system) of the porphyrin−ferrocene SAM cell reported by Uosaki et al.[12a,c] They concluded that the ferrocene and the porphyrin moieties are well-arranged on the gold electrode in the order, the ferrocene and the porphyrin, by using long alkyl spacers between the gold electrode and the ferrocene and between the ferrocene and the porphyrin. Their photocurrent generation mechanism is quite different from our system. The excited singlet state of the porphyrin transfers an electron to MV^{2+} as an electron carrier, followed by the successive hole transfer from the porphyrin to the gold electrode via the ferrocene. Thus, it seems likely that the quantum yield is restricted by the diffusional intermolecular quenching of the excited singlet state of the porphyrin by MV^{2+} via ET, because it must compete with the efficient quenching by the gold electrode via EN.[29] This is in sharp contrast with the present system where the corresponding first step is controllable intramolecular quenching by the C_{60}. In addition, the flexible methylene spacers between the porphyrin and the ferrocene do not allow the comparison between the photodynamics in solutions and in the monolayer on the gold surface.

Ito et al. reported preliminary photodynamical behavior of **2** in various solvents such as benzene, THF, benzonitrile, and DMF.[15i] Nanosecond time-resolved transient absorption spectra of **2b** showed that the characteristic bands due to $C_{60}^{\bullet-}$ appeared at around 700−1100 nm immediately after the excitation of 532 nm laser pulse. In contrast, no apparent absorption due to the zincporphyrin cation radical ($ZnP^{\bullet+}$) was observed within the time resolution (10 ns). In our previous studies on a zincporphyrin−C_{60} dyad with a similar spacer,[15b,c] the rate constant of CS (k_{CS1}) from ^{1}ZnP* to C_{60} is 9.0 × 10^9 s^{-1} in THF and 1.1 × 10^{10} s^{-1} in DMF with quantum yields of 0.94 and 0.95, respectively, whereas the CR rate (k_{CR1}) varies from 2 × 10^9 s^{-1} in THF to >5 × 10^{10} s^{-1} in DMF. The value of k_{CS1} (9.0 × 10^9 s^{-1}) in THF is quite similar to that (1.3 × 10^{10} s^{-1}) of **2b** in THF, which was obtained by the fluorescence lifetime measurements. Based on the results together with the fluorescence studies, one can conclude that initial photoinduced ET from ^{1}ZnP* to C_{60} occurs in **2b**, followed by the fast CSH from the ferrocene to $ZnP^{\bullet+}$ to produce $Fc^{\bullet+}$−ZnP−$C_{60}^{\bullet-}$ within <10 ns (Figure 2). The transient absorption due to the ferrocene cation radical could not be detected because of the small molar absorption coefficient. The lifetime (τ_{CR2}) and the overall quantum yield of $Fc^{\bullet+}$−ZnP−$C_{60}^{\bullet-}$ were reported to be 7.5 μs and 65%, respectively, in benzonitrile, based on the absorption of both the porphyrin and the C_{60}. Given the relative absorption ratio of the porphyrin and the C_{60}, the quantum yield relative to ^{1}ZnP* exceeds 80%. Considering that the CSH is beyond the time resolution of the instrumentation, the rate constant of the charge shift (k_{CSH}) was estimated to be 10^9−10^{11} s^{-1}. It is highly remarkable that both the quantum yield and the lifetime in **2b** are much improved, compared with those of conventional triads[1,2] as well as those of the similar carotenoid (Car)−H_2P−C_{60} triad (τ_{CR2} = 170 ns, Φ = 14% in 2-methyltetrahydrofuran).[16d] This implies that the separation distance between the chromophores and the nature of the spacer are well tuned in **2b**, in addition to the effect of small reorganization energy in C_{60}, as we have proposed.[14b,e,15b,c] Note that as the solvent polarity increased from benzene to DMF, the τ_{CR2} values increased by a factor of 390 (τ_{CR2} = 40 ns in benzene, 3.7 μs in THF, 15.6 μs in DMF). The overall quantum yield of **2b** for CS decreases gradually with a decrease of the solvent polarity from DMF to benzene.[38]

From the above results, the photocurrent generation may be explained by the following mechanism as shown in Figure 7. For the Au/**1b**/O_2(+MV^{2+})/Pt cell, photoinduced ET occurs from ^{1}ZnP* to the C_{60} exclusively. The dominant fluorescence quenching of ^{1}ZnP* by the C_{60} shows that a path of Fc−^{1}ZnP*−C_{60} → $Fc^{\bullet+}$−$ZnP^{\bullet-}$−C_{60} → $Fc^{\bullet+}$− ZnP−$C_{60}^{\bullet-}$ is negligible for the photocurrent generation. On the basis of the redox potential of the excited singlet state of the C_{60} (1.12 V ($^1C_{60}$*/$C_{60}^{\bullet-}$)), it is also possible to generate $Fc-P^{\bullet+}-C_{60}^{\bullet-}$ when the C_{60} is excited. Considering the large difference in molar absorption coefficient between the C_{60} and the porphyrin, the contribution of $^1C_{60}$* for the photocurrent generation would be minor as well. Then the CSH takes place from the ferrocene to $ZnP^{\bullet+}$ to produce $Fc^{\bullet+}$−ZnP−$C_{60}^{\bullet-}$ in the monolayer. The resulting $C_{60}^{\bullet-}$ transfers an electron to diffusing electron carriers such as oxygen (−0.48 V (O_2/$O_2^{\bullet-}$, pH 7.0))[39] and/or MV^{+2} (−0.62 V (MV^{+2}/$MV^{\bullet+}$, pH 7.0)), which eventually give an electron to the counter electrode. On the other hand, the ET rate from the gold electrode to $Fc^{\bullet+}$ is affected by the applied potential to the gold electrode. Thus, as the potential is applied to more negative, the ET rate from the gold electrode to the $Fc^{\bullet+}$ increases, leading to the increase of photocurrent in the system. Overall, it results in the recovery of the initial state and a net vectorial electron flow

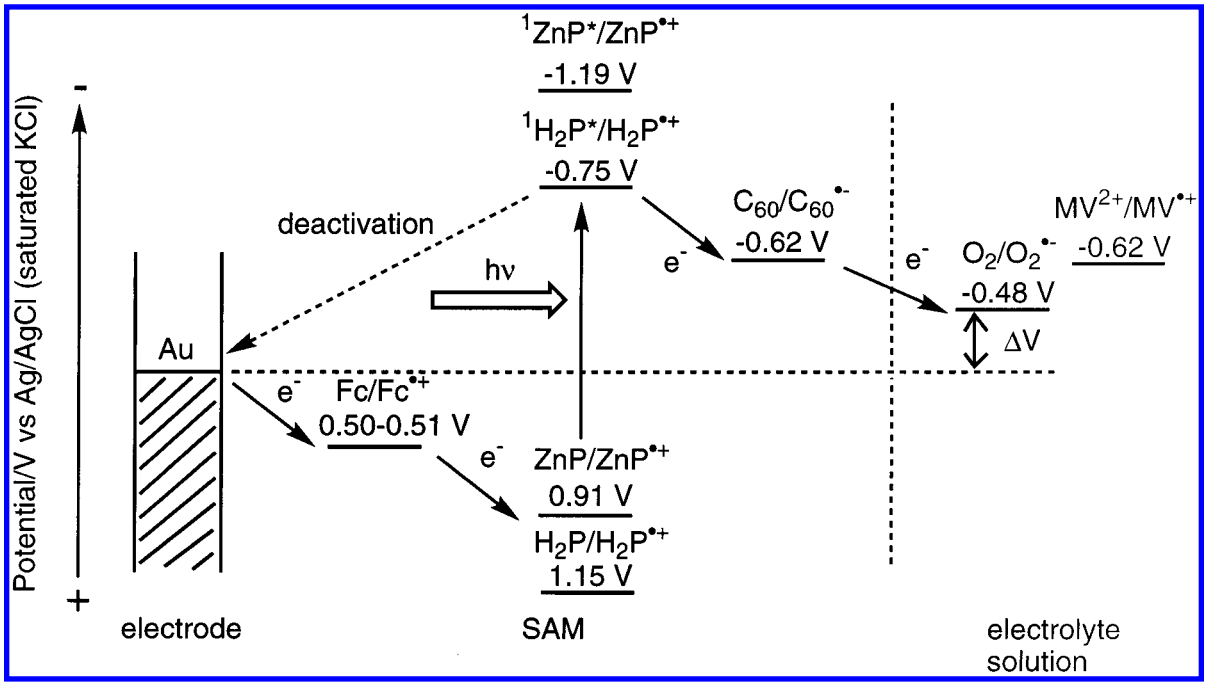

Figure 7. Photocurrent generation mechanism on the basis of the redox potentials.

from the gold electrode to the counter electrode through the monolayer and the electrolyte.

We have shown that, based on the fluorescence lifetime measurements of the porphyrin within the SAM on the gold surface, ^{1}P* is strongly quenched by the gold surface through EN rather than by aggregation of the porphyrins.[23] This implies that initial photoinduced ET from ^{1}P* to the first acceptor must compete with the deactivation due to the gold electrode. Furthermore, the intermolecular CSH from the reduced acceptor to the electron carriers in the electrolyte and the CSH from the Fc to P$^{\bullet+}$ must rival the charge recombination to the ground state. Such processes would reduce the efficiency of CS in the monolayers. The value of the quantum yield ($\Phi_P = 20\%$) for Au/**1b**/O$_2$(+MV^{2+})/Pt cell is positioned between those of the efficiency for the first CS in the monolayer ($\Phi_F = 29\%$) in THF and that ($\Phi_F = 11\%$) in benzene (Table 3). Considering that the long lifetime of the Fc$^{\bullet+}$−P−C$_{60}^{\bullet-}$ state in various solvents, C$_{60}^{\bullet-}$ is quenched completely by electron carriers through diffusional control (5×10^9 M^{-1} s^{-1} × 15×10^{-3} M $= 7.5 \times 10^7$ s^{-1}). Assuming that the quantum yield for the first CS in the monolayer is similar to that for the photocurrent generation, the intermediate value is quite consistent with the assumption that the polarity in the monolayers is similar to those in benzene ($\epsilon = 2.2$) and THF ($\epsilon = 7.58$). Since the overall quantum yield of the triads for CS decreases gradually with a decrease of the solvent polarity,[38] the polarity in the monolayer from **1b** may be a moderate value ($\epsilon = 3\sim7$), which will make the overall value for the CS in the monolayer closer to the quantum yield for the photocurrent generation. Alternatively, if the polarity in the monolayer is similar to that in THF, the moderate efficiency of the CSH from the Fc to ZnP$^{\bullet+}$ would reduce the overall value for the CS in the monolayer, thereby approaching the quantum yield for the photocurrent generation.

Although the quantum yields of these cells are quite similar, the photocurrent generation mechanism in the Au/**1a**/O$_2$-(+MV^{2+})/Pt cell may be different from that in the Au/**1b**/O$_2$-(+MV^{2+})/Pt cell. As we described before, the photodynamical behavior is quite different between zincporphyrin−C$_{60}$ and free base porphyrin−C$_{60}$ dyads. Photoinduced ET generates the ion pair in zinc porphyrin−C$_{60}$ systems, while an exciplex is produced in free base porphyrin−C$_{60}$ systems.[11b] Therefore, for the Au/**1a**/O$_2$(+MV^{2+})/Pt cell, partial CT may occur from ^{1}H$_2$P* to C$_{60}$. However, the complete CT might occur during the subsequent formation of Fc$^{\bullet+}$−H$_2$P−C$_{60}^{\bullet-}$, which is supported by the fact that Fc$^{\bullet+}$−H$_2$P−C$_{60}^{\bullet-}$ is detected in various solvents by nanosecond laser photolysis.[38] Overall, the resulting charge-separated state in the monolayer would produce the cathodic photocurrent, similar to the Au/**1b**/O$_2$(+MV^{2+})/Pt cell. Surprisingly, there is a great discrepancy between the efficiency (1.2−1.6%) for the first CT in the monolayer and the quantum yield (25%) of the Au/**1a**/O$_2$(+MV^{2+})/Pt cell. Considering the small structural difference between **1a** and **1b**, the discrepancy is striking. The reason is not clear at the present, but it might be related to the difference in the initial photodynamics between the free base porphyrin−C$_{60}$ and the zinc porphyrin−C$_{60}$ moieties, as we have already suggested,[11b] and/or the difference in the packing structures of **1a**/Au and **1b**/Au. Otherwise, if the assumption that the polarity in the monolayer is similar to that in THF and benzene is wrong, the discrepancy might be ascribed to the difference in the photodynamics in solutions and the monolayers.

In conclusion, we have developed photoinduced multistep ET systems at the gold electrodes using a combination of SAMs and ferrocene−porphyrin−C$_{60}$ triads. The quantum yields of the triad cells in the three electrode system are 20−25%, which is the highest value ever reported for photoinduced multistep ET at monolayer-modified metal electrodes as well as in artificial membranes using donor−acceptor linked molecules. It should be noted here that utilization of C$_{60}$ with the small reorganization energy satisfies the severe requirement for the photocurrent generation, leading to the high quantum yield even at the metal electrode. Further improvement of the efficiency will be possible by modifying the chromophores, changing the nature of spacer, and selecting suitable substrates as electrodes. Since all of the materials in our system are stable, at least under the experimental conditions, our approach using fullerenes as an acceptor and molecular technologies on substrates using SAMs will provide a new opportunity for the development of molecule-based artificial photosynthetic materials with high efficiencies and molecular devices.

Experimental Section

Materials and Preparation. Synthesis and characterization of **1**−**18** are described in Supporting Information. Gold electrodes (Au/Cr/Si) were prepared by a vacuum deposition technique with chromium (50−100 Å) and gold (100−1000 Å) in a sequence onto a Si (100) wafer (Sumitomo Sitix Corp.), while transparent gold substrates (Au/glass) were made using vacuum deposition of gold (200 Å) onto a transparent glass slide (Matsunami). Atomic force microscopy, scanning tunneling microscopy, and X-ray diffraction studies showed that the gold electrodes have mainly Au(111) surfaces. The roughness factors were estimated to be 1.1 for Au/Cr/Si and 1.5 for Au/glass by iodine chemisorption on the Au(111) surface. The gold-coated wafers (Au/Cr/Si) were cut into slides (ca. 1−3 cm × 1−3 cm), rinsed with dilute hydrochloric acid, Millipore water, and ethanol, and dried with a stream of argon before being soaked in a solution of thiols. The gold substrates on glass (Au/glass) were annealed with hydrogen for 30 s immediately prior to immersion into the solutions. The gold samples were dipped into 50 μM CH_2Cl_2 solution of **1a** at 25 °C for 20 h under argon atmosphere to reach the equilibrium. The solution was shielded from light during the modification. After soaking, **1a**/Au was rinsed well with CH_2Cl_2 and EtOH, and dried with a stream of argon. The surface-bound porphyrins were metalated in 5 mL of $CHCl_3$ solution containing a few drops of MeOH solution saturated with $Zn(OAc)_2$ at 50 °C for 2 h under argon atmosphere. The resulting **1b**/Au was washed copiously with CH_2Cl_2 and EtOH, and dried with a stream of argon. The complete metalation was confirmed using cyclic voltammetry.

Experimental Conditions. UV−visible spectra in solutions were obtained on a Shimadzu UV3000 spectrometer, while those on gold substrates (Au/glass) were recorded on a Hitachi U-3500 spectrometer in transmission mode. Fluorescence spectra in solutions were taken using a Shimadzu RF-1500 spectrofluorophotometer.

The X-ray reflectivity and diffuse scattering measurements were carried out using a high-resolution X-ray diffractometer (Advanced Thin Film X-Ray System ATX-E, Rigaku Corporation).[34] X-rays with wavelength $\lambda = 1.5405$ Å ($CuK_{\alpha 1}$) are generated from a Cu rotating anode (50 kV, 300 mA) and collimated by a parabolic multilayer mirror and monochromator. A divergent slit (0.1 × 10 mm^2) was utilized to control the exposure area on the sample surface, and a couple of receiving slits (0.2 × 15 mm^2) were mounted in front of a NaI crystal scintillation counter. Specular reflectivity curves were recorded using ω-2Θ scans with Θ ranging from 0° to 4°. Diffuse scattering data were measured via ω-2Θ scans with 2Θ fixed at from 0.55° to 1.65°. Area mapping around (000) reciprocal lattice point was used for qualitative analysis, and separate Θ-scans were fitted precisely. Experimental data were analyzed by theoretical simulations using the Levenberg−Marquardt method to solve the nonlinear least-squares problem.

All electrochemical studies were performed on a Bioanalytical Systems, Inc. CV-50W voltammetric analyzer using a standard three-electrode cell with a modified Au working electrode (0.48 cm^2), a platinum wire counter electrode, and a Ag/AgCl (saturated KCl) reference electrode. Photoelectrochemical measurements were carried out in a one-compartment Pyrex UV cell (5 mL) under argon atmosphere. The cell was illuminated with monochromatic excitation light through interference filters (MIF−S, Vacuum Optics Corporation of Japan) by a 180 W UV lamp (Sumida LS-140UV) on the SAM of 0.48 cm^2. Unless otherwise stated, an O_2-saturated 0.1 M Na_2SO_4 aqueous electrolyte solution was used. The photocurrent was measured in a three-electrode arrangement, a modified gold working electrode, a platinum wire counter electrode (the distance between the electrodes is 0.3 mm), and a Ag/AgCl (saturated KCl) reference. The light intensity was monitored by an Anritsu ML9002A optical power meter.

Acknowledgment. We are grateful to Kazuhiko Omote (X-ray Research Laboratory, Rigaku Corporation, Tokyo, Japan) for the measurements of the monolayer thickness. We thank Dr. Kiminori Ushida (the Institute of Physical and Chemical Research) for his helpful advice and comments. This work was supported by Grant-in-Aids for COE Research and Scientific Research on Priority Area of Electrochemistry of Ordered Interfaces (No.11118247 to H.I.) and Creation of Delocalized Electronic Systems (No.10146103 to Y.S.) from Ministry of Education, Science, Sports and Culture, Japan. Y.S. and H.I. thank the Mitsubishi Foundation and Sumitomo Foundation for financial support.

Supporting Information Available: The synthesis and characterization of **1**−**18** and the experimental details. This material is available free of charge via the Internet at http://pubs.acs.org.

References and Notes

(1) *In the Photosynthetic Reaction Center*; Deisenhofer, J., Norris, J. R., Eds.; Academic Press: San Diego, 1993.

(2) (a) Connolly, J. S.; Bolton, J. R. In *Photoinduced Electron Transfer*; Fox, M. A., Chanon, M., Eds.; Elsevier: Amsterdam, 1988; Part D, pp 303−393. (b) Wasielewski, M. R. In *Photoinduced Electron Transfer*; Fox, M. A., Chanon, M., Eds.; Elsevier: Amsterdam, 1988; Part A, pp 161−206. (c) Wasielewski, M. R. *Chem. Rev.* **1992**, *92*, 435. (d) Gust, D.; Moore, T. A.; Moore, A. L. *Acc. Chem. Res.* **1993**, *26*, 198. (e) Paddon-Row, M. N. *Acc. Chem. Res.* **1994**, *27*, 18. (f) Kurreck, H.; Huber, M. *Angew. Chem., Int. Ed. Engl.* **1995**, *34*, 849. (g) Osuka, A.; Mataga, N.; Okada, T. *Pure Appl. Chem.* **1997**, *69*, 797.

(3) (a) Seta, P.; Bienvenue, E.; Moore, A. L.; Mathis, P.; Bensasson, R. V.; Liddell, P. A.; Pessiki, P. J.; Joy, A.; Moore, T. A.; Gust, D. *Nature* **1985**, *316*, 653. (b) Steinberg-Yfrach, G.; Liddell, P. A.; Hung, S.-C.; Moore, A. L.; Gust, D.; Moore, T. A. *Nature* **1997**, *385*, 239. (c) Steinberg-Yfrach, G.; Rigaud, J.-L.; Durantini, E. N.; Moore, A. L.; Gust, D.; Moore, T. A. *Nature* **1998**, *392*, 479.

(4) Fujihira, M. *Mol. Cryst. Liq. Cryst.* **1990**, *183*, 59.

(5) Sakata, Y.; Tatemitsu, H.; Bienvenue, E.; Seta, P. *Chem. Lett.* **1988**, 1625.

(6) Deronzier, A.; Essakalli, M. *J. Phys. Chem.* **1991**, *95*, 1737.

(7) Wang, X. D.; Zhang, B. W.; Bai, J. W.; Cao, Y.; Xiao, X. R.; Xu, J. M. *J. Phys. Chem.* **1992**, *96*, 2886.

(8) Liang, K.; Law, K.-Y.; Whitten, D. G. *J. Phys. Chem. B*, **1997**, *101*, 540.

(9) Tkachenko, N. V.; Tauber, A. Y.; Hynninen, P. H.; Sharonov, A. Y.; Lemmetyinen, H. *J. Phys. Chem. A* **1999**, *103*, 3657.

(10) *In An Introduction to Ultrathin Organic Films*; Ulman, A., Ed.; Academic Press: San Diego, 1991.

(11) (a) Akiyama, T.; Imahori, H.; Ajavakom, A.; Sakata, Y. *Chem. Lett.* **1996**, 907. (b) Imahori, H.; Ozawa, S.; Ushida, K.; Takahashi, M.; Azuma, T.; Ajavakom, A.; Akiyama, T.; Hasegawa, M.; Taniguchi, S.; Okada, T.; Sakata, Y. *Bull. Chem. Soc. Jpn.* **1999**, *72*, 485.

(12) (a) Uosaki, K.; Kondo, T.; Zhang, X.-Q.; Yanagida, M. *J. Am. Chem. Soc.* **1997**, *119*, 8367. (b) Kondo, T.; Yanagida, M.; Nomura, S.-i.; Ito, T.; Uosaki, K. *J. Electroanal. Chem.* **1997**, *438*, 121. (c) Kondo, T.; Kanai, T.; Iso-o, K.; Uosaki, K. *Z. Phys. Chem.* **1999**, *212*, 23.

(13) (a) Koide, Y.; Terasaki, N.; Akiyama, T.; Yamada, S. *Thin Solid Films* **1999**, *350*, 223. (b) Lahav, M.; Gabriel, T.; Shipway, A. N.; Willner, I. *J. Am. Chem. Soc.* **1999**, *121*, 258.

(14) (a) Jensen, A. W.; Wilson, S. R.; Schuster, D. I. *Bioorg. Med. Chem.* **1996**, *4*, 767. (b) Imahori, H.; Sakata, Y. *Adv. Mater.* **1997**, *9*, 537. (c) Gust, D.; Moore, T. A.; Moore, A. L. *Res. Chem. Intermed.* **1997**, *23*, 621. (d) Martín, N.; Sánchez, L.; IIIescas, B.; Pérez, I. *Chem. Rev.* **1998**, *98*, 2527. (e) Imahori, H.; Sakata, Y. *Eur. J. Org. Chem.* **1999**, 2445.

(15) (a) Imahori, H.; Hagiwara, K.; Akiyama, T.; Taniguchi, S.; Okada, T.; Sakata, Y. *Chem. Lett.* **1995**, 265. (b) Imahori, H.; Hagiwara, K.; Aoki, M.; Akiyama, T.; Taniguchi, S.; Okada, T.; Shirakawa, M.; Sakata, Y. *J. Am. Chem. Soc.* **1996**, *118*, 11771. (c) Imahori, H.; Hagiwara, K.; Akiyama, T.; Aoki, M.; Taniguchi, S.; Okada, T.; Shirakawa, M.; Sakata, Y. *Chem. Phys. Lett.* **1996**, *263*, 545. (d) Imahori, H.; Yamada, K.; Hasegawa, M.;

Taniguchi, S.; Okada, T.; Sakata, Y. *Angew. Chem., Int. Ed. Engl.* **1997**, *36*, 2626. (e) Higashida, S.; Imahori, H.; Kaneda, T.; Sakata, Y. *Chem. Lett.* **1998**, 605. (f) Tamaki, K.; Imahori, H.; Nishimura, Y.; Yamazaki, I.; Shimomura, A.; Okada, T.; Sakata, Y. *Chem. Lett.* **1999**, 227. (g) Tamaki, K.; Imahori, H.; Nishimura, Y.; Yamazaki, I.; Sakata, Y. *Chem. Commun.* **1999**, 625. (h) Imahori, H.; Yamada, H.; Ozawa, S.; Ushida, K.; Sakata, Y. *Chem. Commun.* **1999**, 1165. (i) Fujitsuka, M.; Ito, O.; Imahori, H.; Yamada, K.; Yamada, H.; Sakata, Y. *Chem. Lett.* **1999**, 721. (j) Yamada, K.; Imahori, H.; Nishimura, Y.; Yamazaki, I.; Sakata, Y. *Chem. Lett.*, **1999**, 895.

(16) (a) Liddell, P. A.; Sumida, J. P.; Macpherson, A. N.; Noss, L.; Seely, G. R.; Clark, K. N.; Moore, A. L.; Moore, T. A.; Gust, D. *Photochem. Photobiol.* **1994**, *60*, 537. (b) Imahori, H.; Cardoso, S.; Tatman, D.; Lin, S.; Noss, L.; Seely, G. R.; Sereno, L.; de Silber, J. C.; Moore, T. A.; Moore, A. L.; Gust, D. *Photochem. Photobiol.* **1995**, *62*, 1009. (c) Kuciauskas, D.; Lin, S.; Seely, G. R.; Moore, A. L.; Moore, T. A.; Gust, D.; Drovetskaya, T.; Reed, C. A.; Boyd, P. D. W. *J. Phys. Chem.* **1996**, *100*, 15926. (d) Liddell, P. A.; Kuciauskas, D.; Sumida, J. P.; Nash, B.; Nguyen, D.; Moore, A. L.; Moore, T. A.; Gust, D. *J. Am. Chem. Soc.* **1997**, *119*, 1400. (e) Kuciauskas, D.; Liddell, P. A.; Lin, S.; Johnson, T. E.; Weghorn, S. J.; Lindsey, J. S.; Moore, A. L.; Moore, T. A.; Gust, D. *J. Am. Chem. Soc.* **1999**, *121*, 8604.

(17) (a) Williams, R. M.; Zwier, J. M.; Verhoeven, J. W. *J. Am. Chem. Soc.* **1995**, *117*, 4093. (b) Lawson, J. M.; Oliver, A. M.; Rothenfluh, D. F.; An, Y.-Z.; Ellis, G. A.; Ranasinghe, M. G.; Khan, S. I.; Franz, A. G.; Ganapathi, P. S.; Shephard, M. J.; Paddon-Row, M. N.; Rubin, Y. *J. Org. Chem.* **1996**, *61*, 5032. (c) Williams, R. M.; Koeberg, M.; Lawson, J. M.; An, Y.-Z.; Rubin, Y.; Paddon-Row, M. N.; Verhoeven, J. W. *J. Org. Chem.* **1996**, *61*, 5055. (d) Bell, T. D. M.; Smith, T. A.; Ghiggino, K. P.; Ranasinghe, M. G.; Shephard, M. J.; Paddon-Row, M. N. *Chem. Phys. Lett.* **1997**, *268*, 223.

(18) (a) Sariciftci, N. S.; Wudl, F.; Heeger, A. J.; Maggini, M.; Scorrano, G.; Prato, M.; Bourassa, J.; Ford, P. C. *Chem. Phys. Lett.* **1995**, *247*, 510. (b) Guldi, D. M.; Maggini, M.; Scorrano, G.; Prato, M. *J. Am. Chem. Soc.* **1997**, *119*, 974. (c) Maggini, M.; Guldi, D. M.; Mondini, S.; Scorrano, G.; Paolucci, F.; Ceroni, P.; Roffia, S. *Chem. Eur. J.* **1998**, *4*, 1192. (d) Polese, A.; Mondini, S.; Bianco, A.; Toniolo, C.; Scorrano, G.; Guldi, D. M.; Maggini, M. *J. Am. Chem. Soc.* **1999**, *121*, 3446. (e) Maggini, M.; Guldi, D. M.; Mondini, S.; Scorrano, G.; Paolucci, F.; Ceroni, P.; Roffia, S. *Chem. Eur. J.* **1998**, *4*, 1992.

(19) (a) Nakamura, Y.; Minowa, T.; Hayashida, Y.; Tobita, S.; Shizuka, H.; Nishimura, J. *J. Chem. Soc., Faraday Trans.* **1996**, *92*, 377. (b) Baran, P. S.; Monaco, R. R.; Khan, A.; Schuster, D. I.; Wilson, S. R. *J. Am. Chem. Soc.* **1997**, *119*, 8363. (c) Armaroli, N.; Diederlich, F.; Dietrich-Buchecker, C. O.; Flamigni, L.; Marconi, G.; Nierengarten, J.-F.; Sauvage, J.-P. *Chem. Eur. J.* **1998**, *4*, 406. (d) Armspach, D.; Constable, E. C.; Diederich, F.; Housecroft, C. E.; Nierengarten, J.-F. *Chem. Eur. J.* **1998**, *4*, 723. (e) Tkachenko, N. V.; Rantala, L.; Tauber, A. Y.; Helaja, J.; Hynninen, P. H.; Lemmetyine, H. *J. Am. Chem. Soc.* **1999**, *121*, 9378.

(20) Guldi, D. M.; Asmus, K.-D. *J. Am. Chem. Soc.* **1997**, *119*, 5744.

(21) McCallien, D. W. J.; Burn, P. L.; Anderson, H. L. *J. Chem. Soc., Perkin Trans. 1*, **1997**, 2581.

(22) (a) Sondag-Huethorst, J. A. M.; Schönenberger, C.; Fokkink, L. G. F. *J. Phys. Chem.* **1994**, *98*, 6826. (b) Poirier, G. E. *Langmuir* **1997**, *13*, 2019. (c) Poirier, G. E. *Chem. Rev.* **1997**, *97*, 1117.

(23) (a) Imahori, H.; Norieda, H.; Ozawa, S.; Ushida, K.; Yamada, H.; Azuma, T.; Tamaki, K.; Sakata, Y. *Langmuir* **1998**, *14*, 5335. (b) Imahori, H.; Norieda, H.; Nishimura, Y.; Yamazaki, I.; Higuchi, K.; Kato, N.; Motohiro, T.; Yamada, H.; Tamaki, K.; Arimura, M.; Sakata, Y. *J. Phys. Chem. B*, in press.

(24) (a) Zak, J.; Yuan, H.; Ho, M.; Woo, L. K.; Porter, M. D. *Langmuir* **1993**, *9*, 2772. (b) Shimazu, K.; Takeuchi, M.; Fujii, H.; Suzuki, M.; Saiki, H.; Yoshimura, T.; Uosaki, K. *Thin Solid Films* **1996**, *273*, 250. (c) Hutchison, J. E.; Postlethwaite, T. A.; Chen, C.-h.; Hathcock, K. W.; Ingram, R. S.; Ou, W.; Linton, R. W.; Murray, R. W. *Langmuir* **1997**, *13*, 2143.

(25) (a) Dick, H. A.; Bolton, J. R.; Picard, G.; Munger, G.; Leblanc, R. M. *Langmuir* **1988**, *4*, 133. (b) Schick, G. A.; Schreiman, I. C.; Wagner, R. W.; Lindsey, J. S.; Bocian, D. F. *J. Am. Chem. Soc.* **1989**, *111*, 1344. (c) Gust, D.; Moore, T. A.; Moore, A. L.; Luttrull, D. K.; DeGraziano, J. M.; Boldt, N. J.; Auweraer, M. V.; de Schryver, F. C. *Langmuir* **1991**, *7*, 1483. (d) Choudhury, B.; Weedon, A. C.; Bolton, J. R. *Langmuir* **1998**, *14*, 6192. (e) Choudhury, B.; Weedon, A. C.; Bolton, J. R. *Langmuir* **1998**, *14*, 6199.

(26) (a) Akins, D. L.; Özçelik, S.; Zhu, H.-R.; Guo, C. *J. Phys. Chem.* **1996**, *100*, 14390. (b) Maiti, N. C.; Mazumdar, S.; Periasamy, N. *J. Phys. Chem. B* **1998**, *102*, 1528. (c) Khairrutdinov, R. F.; Serpone, N. *J. Phys. Chem. B* **1999**, *103*, 761.

(27) Kasha, M. *Radiat. Res.* **1963**, *20*, 55.

(28) Osuka, A.; Maruyama, K. *J. Am. Chem. Soc.* **1988**, *110*, 4454.

(29) (a) Chance, R. R.; Prock, A.; Silbey, R. *Adv. Chem. Phys.* **1978**, *37*, 1. (b) Waldeck, D. H.; Alivisatos, A. P.; Harris, C. B. *Surf. Sci.* **1985**, *158*, 103. (c) Zhou, X.-L.; Zhu, X.-Y.; White, J. M. *Acc. Chem. Res.* **1990**, *23*, 327. (d) Cnosse, G.; Drabe, K. E.; Wiersma, D. A. *J. Chem. Phys.* **1993**, *98*, 5276. (d) Barnes, W. L. *J. Mod. Opt.* **1998**, *45*, 661.

(30) Robert, G. *Langmuir*−*Blodgett films*; Plenum Press: New York, 1990.

(31) (a) Imahori, H.; Azuma, T.; Ozawa, S.; Yamada, H.; Ushida, K.; Ajavakom, A.; Norieda, H.; Sakata, Y. *Chem. Commun.* **1999**, 557. (b) Imahori, H.; Azuma, T.; Ajavakom, A.; Norieda, H.; Yamada, H.; Sakata, Y. *J. Phys. Chem. B* **1999**, *103*, 7233.

(32) (a) Shi, X.; Caldwell, W. B.; Chen, K.; Mirkin, C. A. *J. Am. Chem. Soc.* **1994**, *116*, 11598. (b) Arias, F.; Godínez, L. A.; Wilson, S. R.; Kaifer, A. E.; Echegoyen, L. *J. Am. Chem. Soc.* **1996**, *118*, 6086. (c) Mirkin, C. A.; Caldwell, W. B. *Tetrahedron* **1996**, *52*, 5113.

(33) Porter, M. D.; Bright, T. B.; Allara, D. L.; Chidsey, C. E. D. *J. Am. Chem. Soc.* **1987**, *109*, 3559.

(34) Ulyanenkov, A.; Omote, K.; Matsuo, R.; Harada, J.; Matsuno, S.-Y. *J. Phys. D: Appl. Phys.* **1999**, *32*, 1.

(35) (a) Kim, Y.-S.; Liang, K.; Law, K.-Y.; Whitten, D. G. *J. Phys. Chem.* **1994**, *98*, 984. (b) Wu, D.-G.; Huang, C.-H.; Gan, L.-B.; Zhang, W.; Zheng, J.; Luo, H. X.; Li, N. Q. *J. Phys. Chem. B* **1999**, *103*, 4377.

(36) Aoki, A.; Abe, Y.; Miyashita, T. *Langmuir* **1999**, *15*, 1463.

(37) (a) Hwang, K. C.; Mauzerall, D. *Nature* **1993**, *361*, 138. (b) Niu, S.; Mauzerall, D. *J. Am. Chem. Soc.* **1996**, *118*, 5791. (c) Luo, C.; Huang, C.; Gan, L.; Zhou, D.; Xia, W.; Zhuang, Q.; Zhao, Y.; Huang, Y. *J. Phys. Chem.* **1996**, *100*, 16685.

(38) Fujitsuka, M.; Ito, O., private communication.

(39) In *Standard Potentials in Aqueous Solution*; Bard, A. J., Rarsons, R., Jordan, J., Eds.; Marcel Dekker: New York, 1985.